Electronic Supplementary Material (ESI) for Journal of Materials Chemistry A.

—Electronic Supplementary Information— Zirconia-free NaSICON Solid Electrolyte Materials for Sodium All-solid-state Batteries

Aaron Jue Kang Tieu[1#], Eunike Mahayoni[2,3#], Yuheng Li[1], Zeyu Deng[1], François Fauth[4], Jean-Noël Chotard[2,3], Vincent Seznec[2,3], Stefan Adams[1▲], Christian Masquelier[2,3,5†], Pieremanuele Canepa[1,6,7*]

[1]Department of Materials Science and Engineering, National University of Singapore, College of Design and Engineering, Singapore 117575

[2]Laboratoire de Réactivité et de Chimie des Solides (LRCS), CNRS UMR 7314, Université de Picardie Jules Verne, 80039 Amiens Cedex, France

[3]RS2E, Réseau Français sur le Stockage Electrochimique de l'Energie, FR CNRS 3459, F-80039 Amiens Cedex 1, France

[4]CELLS-ALBA Synchrotron, Cerdanyola del Vallès, E-08290 Barcelona, Spain

[5]ALISTORE-ERI European Research Institute, FR CNRS 3104, Amiens, F-80039 Cedex 1, France

[6]Department of Electrical and Computer Engineering, Houston, Texas 77204, United States

[7]Texas Center for Superconductivity, University of Houston, Houston, TX, 77204, USA

▲E-mail: mseasn@nus.edu.sg
†E-mail: christian.masquelier@u-picardie.fr
*E-mail: pcanepa@uh.edu

#These authors contributed equally

S1 Characterization of NaSICON materials

Synthesis of $Na_3V_2(PO_4)_3$ electrode material: The electrode active material $Na_3V_2(PO_4)_3$ (NVP) is synthesized via solid-state reaction[1]. NH_4VO_3 (99%, Sigma-Aldrich) and NaH_2PO_4 (99%, Sigma-Aldrich) were mixed in water at 333 K overnight where the solvent was evaporated slowly. The mixture was then slowly heated to 573 K under air to mitigate the volumetric expansion from the heating process. The resulting dried mixture was ground into powder and calcinated at 673 K for 5 hours under a reducing atmosphere (Ar : H_2 = 90 : 10 vol%), followed by 1023 K for 12 hours under the same atmosphere when the green powder of $Na_3V_2(PO_4)_3$ is obtained.

Powder X-Ray Diffraction: Patterns of Powder X-Ray diffraction (PXRD) of the relevant NZSP materials were measured at ~25°C (~298 K) using a Bruker D8 Advance diffractometer with a copper source ($K_{\alpha1}$ = 1.54056 Å and $K_{\alpha2}$ = 1.54439 Å), and a step size of 0.021°.

For variable temperature XRD measurement, XRD of the NZSP material was carried out over a temperature range of 303 K to 573 K, with a heating step size of 10 K increment for each succeeding diffraction pattern. A temperature ramping of 10 K per minute to the next temperature, followed by a holding time of 15 minutes was done according to the set program before each diffraction pattern was taken. The diffraction pattern was obtained using a PANalytical X'Pert Pro Diffractometer equipped with an Anton Paar HTK 1200 high-temperature camera, with a copper source ($K_{\alpha1}$ = 1.54056 Å and $K_{\alpha2}$ = 1.54439 Å) and a step size of 0.021°.

Synchrotron Powder X-ray Diffraction: Synchrotron PXRD measurements of the L15 NZSP sample were performed on the MSPD beamline of the ALBA synchrotron in Spain[2] using a Debye−Scherrer geometry (λ = 0.4437 Å). All Rietveld refinements for all diffraction patterns of both synchrotron and laboratory PXRD experiments were performed using FullProf[3] software.

Thermogravimetric Analysis measurements: Thermogravimetric analysis (TGA) of $ZrO(NO_3)_2 . xH_2O$ was done using TA Instruments Q50 Thermogravimetric Analyzer to detect the amount of Zr in the precursor to be put into the synthesis, as well as the water content. The measurement was done in a nitrogen (N_2) atmosphere, from 298 K to 1223 K with a heating step of 5 K per minute in an alumina crucible. Approximately 30 mg of $ZrO(NO_3)_2 . xH_2O$ precursor was used for the TGA.

Differential Scanning Calorimetry: Differential scanning calorimetry (DSC) of the L15 NZSP sample was done using the NETZSCH DSC 204 F1 calorimeter. Approximately 11.8 mg of L15 was used, measured in a standard Aluminium (Al) crucible, with a heating/cooling range of 263 K to 523 K, with a heating/cooling ramp of 10 K/min.

Inductive Coupled Plasma Spectroscopy of NZSP: Elemental analysis was performed with Inductive Coupled Plasma Optical Emission Spectroscopy (ICP-OES) through a Perkin Elmer Avio 500 ICP Spectrometer. Approximately 20 mg of the sintered NZSP sample was ground to a fine powder and digested in a mixture of HNO_3, HCl, and HF (with a 1 : 3 : 1 ratio) on a hotplate for 2 hours. Then, the mixture was topped up the mixture with deionized water. A clear solution was observed before ICP-OES analysis.

Raman spectroscopy: The experimental spectra of the synthesized NZSP samples and other compounds of interest (see main text) were obtained using a 514 nm Argon laser from LabRam HR Evolution and a Raman spectrometer from Horiba Scientific. Spectra were acquired from 100 cm^{-1} to 2000 cm^{-1}.

Fingerprinting Raman Spectra via Density Functional Theory: Representative Na-vacancies and P/Si ordering of $Na_3Zr_2Si_2PO_{12}$ (N3.0ZSP) were generated from the predicted phase diagram of Ref. 23. The simulated Raman spectra of $Na_3Zr_2Si_2PO_{12}$ (N3.0ZSP), *m*-ZrO_2, $Na_2ZrSi_2O_7$, and Na_3PO_4 were obtained using density functional theory as implemented in the CRYSTAL17 code[4]. In CYSTAL17, the crystalline wavefunctions were expanded using a linear combination of atomic orbitals described by all-electrons Gaussian basis set: for Na[5] a 8-511G, for Si a 88-31-G(*)[6], and for P a 85-21-G(*), and for O a 8-411G(*), and reported in **Table S11** of the Supplementary Information. Zr atoms were described using an effective core potential by Hay and Wadt[7] excluding the semicore *4s* and *4p* states, whereas the valence electrons were treated with a 311G31*d* basis set[8]. In these DFT simulations, the unknown exchange-correlation functional was approximated by the PBE0 hybrid functional proposed by Adamo and Barone[9]. PBE0 includes 25% of the exact Hartree Fock (HF) exchange[10]. The DFT total energies were converged using a homogenous *k*-point grid of 7x7x7 (SHRINK: 7 7). With these settings, the total energies were considered to converge within 10^{-11} eV/cell. Within these settings stated above, all structures were fully relaxed (coordinates, shape, volume, and lattice constants). The prediction of the Raman intensities was achieved using the coupled perturbed Kohn–Sham theory, enabling the computation of the third-order derivatives of the DFT total energy with respect to the applied directions of the electric field[10-12].

Scanning Electron Microscopy and Energy Dispersive X-Ray Spectroscopy: The microstructures of the sintered pellets used for the electrochemical impedance measurements were analyzed using the secondary electron mode implemented in a Supra40 (Zeiss) scanning electron microscope (SEM). The energy dispersive X-Ray spectroscopy (EDS) was performed using the Oxford Ultima Max EDS. The incident electrons of the SEM and EDS measurements were carried out using a 10 kV accelerating voltage. Samples were handled in air. The detection of grains from the micrographs of the cross-section of the pellet was through a methodology developed in Ref. 32 in the main text.

Electrochemical Impedance Spectroscopy measurements: Sintered pellets were gold-sputtered (~75 nm) with a coater (Bal-Tec SCD 050 Sputter Coater). A vacuum / Ar charge was repeated three times before sputtering. A beam current of 20 mA was applied, and the sputtering lasted ~120 s for each side of the pellet. Carbon paper was then added to each side of the pellet to facilitate good electrical contact with the current collectors for the impedance measurements. For the low-temperature measurements (173 K to 253 K), we employed a cell immersed in a Janis STVP-200-Sol Cryostat connected to a Solartron 1260 A/Solartron 1296 dielectric interface. For moderate-temperature measurements (273 K to 413 K), a CESH cell holder in the ITS instrument setup from Bio-Logic was used. The CESH cell was loaded into the ITS instrument. For high temperature (433 K to 573 K) measurements, a cell holder from Bio-Logic Instruments HTF-1100 setup was used as the sample holder cell. The impedance measurements were performed with a Bio-Logic MTZ-35 Impedance analyzer on a two-wire setup connected to either of the sample holders. Sample loading took place in open air and at

room temperature. Impedance spectra were sampled in a frequency range from 10 MHz to 1 Hz (20 points per decade of frequency), with an alternating voltage amplitude of ±20 mV.

The formula for calculating the total ionic conductivity is as follows:

$$\sigma_{total} = \frac{l}{R_{total}A}$$

where σ_{total} is the total ionic conductivity in S cm^{-1}, l is the thickness of the sample in cm, R_{total} is the total resistance experienced by the pellet in Ohms, and A is the surface area in contact with the current collector, in cm^2.

Battery assembly and measurements: The NVP | NZSP-L0 | NVP and NVP | NZSP-L15 | NVP symmetric all-solid-state batteries are assembled in a 10 mm carbon die and sintered via Spark Plasma Sintering (SPS) at 1173 K, 8 kN, 15 minutes holding time. The cathode part contains 20 mg NVP, 48 mg NZSP (L0/L15), and 12 mg C-45 (Sigma-Aldrich). The mass of the separator layer is 60 mg. The anode part contains 40 mg NVP, 96 mg NZSP (L0/15), and 24 mg C-45. The obtained symmetric cell was placed inside a high-temperature cell (described in Figure S18) and cycled at high temperatures in a tubular furnace.

S2 Thermogravimetric Analysis

Figure S1: Thermogravimetric analysis of $ZrO(NO_3)_2 \cdot xH_2O$ to determine the amount of Zr available in the precursor, as well as its water content. The heating rate is 5 K per minute, in nitrogen (N_2) atmosphere, from 298 K to 1223 K. Approximately 30 mg was used for the TGA.

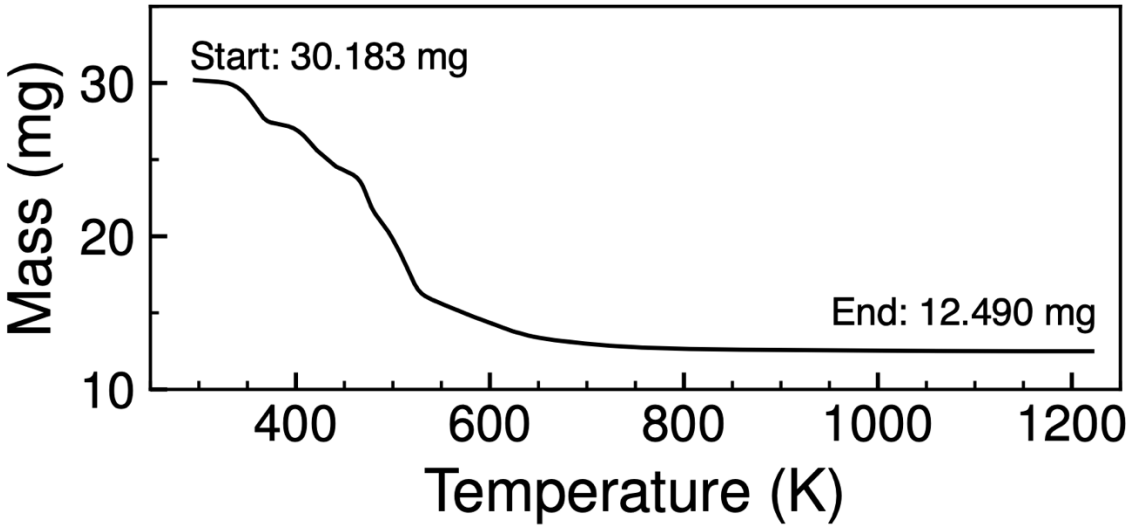

S3 Elemental Analysis

Table S2: Elemental analysis with ICP-OES of the L15 sample. ~20 mg of sintered L15 sample was grounded up to a fine powder, and digested on a mixture of HNO_3, HCl, and HF in a ratio of 1 : 3 : 1 on a hotplate for 2 hours. The mixture was then topped up with deionized water. A clear solution was observed prior to analysis. The ratios are normalized to Si + P = 3.000.

	Na	**Zr**	**Si**	**P**
%w/w	15.35	28.69	12.46	3.33
Ratio	3.634	1.711	2.414	0.586

Table S3: Weight percentages of the phases after Rietveld refinement with the FullProf software. The phases used to index the peaks were N3.4ZSP ($C2/c$), *m*-ZrO_2 ($P2/c$), Na2ZrSi2O7 ($P\bar{1}$), and Na3PO4 ($P\bar{4}2_1c$).

Sample	**N3.4ZSP**	***m*-ZrO_2**	**$Na_2ZrSi_2O_7$**	**Na_3PO_4**
L0	92.07	7.93	–	–
L5	96.28	3.72	–	–
L10	97.35	2.65	–	–
L15	100	–	–	–
L20	99.16	–	–	0.84
L25	94.50	–	4.67	0.83

S4 Rietveld Refinement of Synchrotron Powder X-Ray Diffraction

Table S4: Atomic coordinates, U_{ISO}, and Wyckoff number of the refined L15 cell derived from the Rietveld refinement of the synchrotron PXRD pattern reported in Figure 1c. FullProf software performed the Rietveld refinement to obtain these coordinates and parameters.

Species	Wyckoff	x	y	z	U_{iso}	Occ.
Zr	8f	0.10120	0.25120	0.05680	0.00380	1.0
P1	4e	0.00000	0.03900	0.25000	0.00070	0.2
P2	8f	0.35950	0.10700	0.26200	0.00070	0.2
Si1	4e	0.00000	0.03900	0.25000	0.00070	0.8
Si2	8f	0.35950	0.10700	0.26200	0.00070	0.8
O1	8f	0.14800	0.42900	0.22800	0.00000	1.0
O2	8f	0.43400	0.45300	0.08400	0.00000	1.0
O3	8f	0.25300	0.18600	0.21500	0.00000	1.0
O4	8f	0.37300	0.13600	0.10300	0.00000	1.0
O5	8f	0.45000	0.17600	0.43600	0.00000	1.0
O6	8f	0.07400	0.14400	0.23600	0.00000	1.0
Na(1)	4d	0.25000	0.25000	0.50000	0.28476	1.0
Na(2)	4e	0.50000	0.89400	0.25000	0.00000	1.0
Na(3)	8f	0.83200	0.08500	0.80300	0.08218	0.7

Figure S5: PXRD patterns (from bench XRD) of the L15 NaSICON sample in the temperature range from 303 K to 573 K, and a temperature step of 10 K. Measurement was conducted using a PANalytical X'Pert Pro Diffractometer equipped with an Anton Paar HTK 1200 high-temperature camera, with a copper source ($K_{\alpha1}$ = 1.54056 Å and $K_{\alpha2}$ = 1.54439 Å) and a step size of 0.021°. (a) PXRD patterns of the L15 NaSICON sample were recorded from 303 K to 573 K, with a temperature step of 10 K. Peak evolution of NaSICON peak with respect to temperature at 2θ angles between 18.6 – 19.6° (b), 22 – 23° (c), and 26.6 – 27.8° (d).

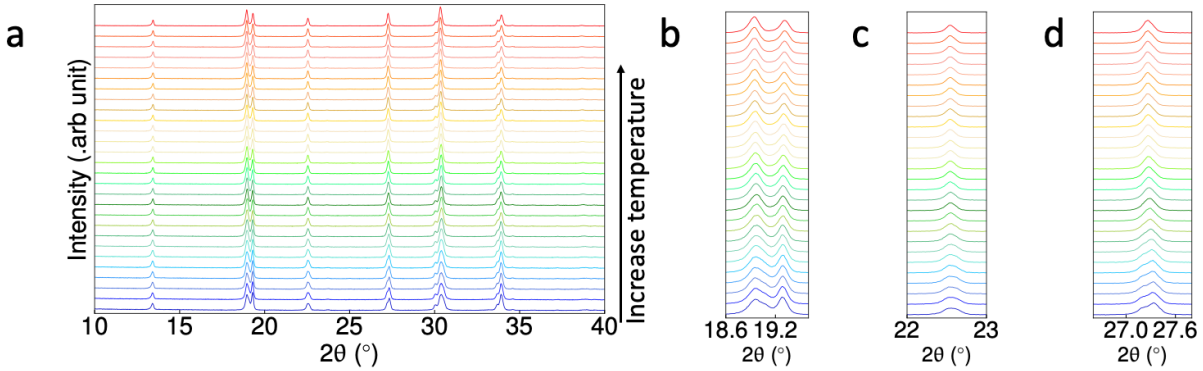

S5 Differential Scanning Calorimetry

Figure S6: DSC measurements of the L15 NaSICON sample. Approximately 11.8 mg of the grounded sample was used to measure the DSC. The measurements were taken from 243 K to 573 K, with a heating/cooling step of 10 K per minute.

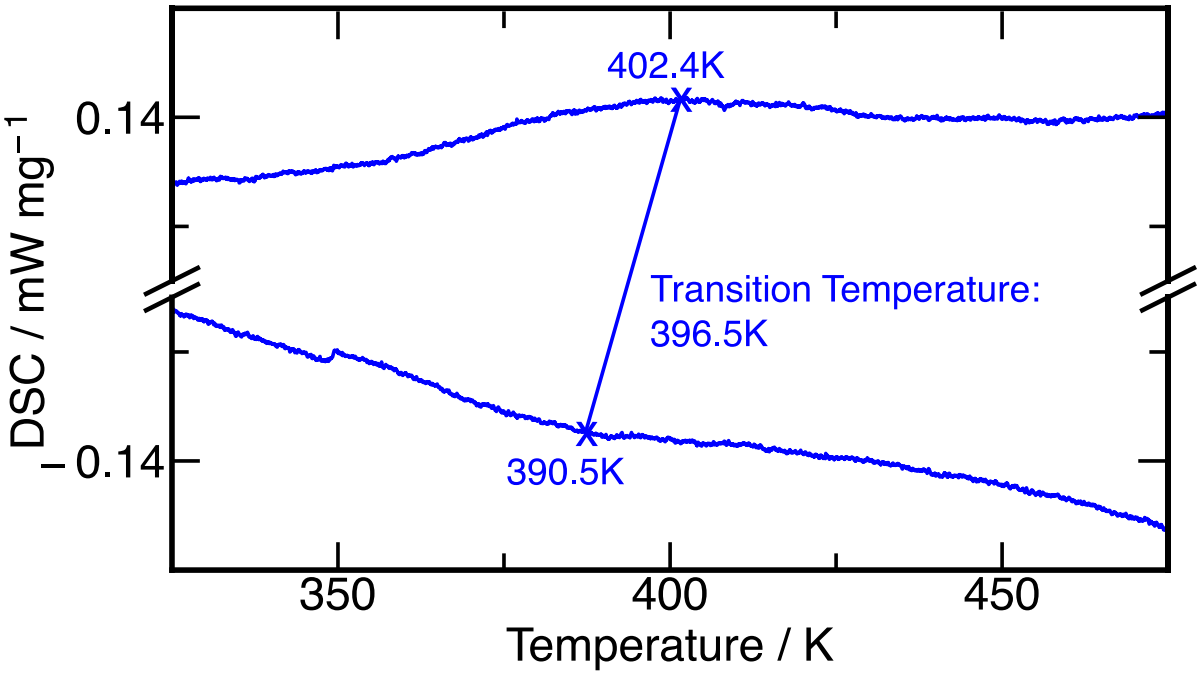

S6 Raman Assignment via Density Functional Theory

Table S7: Assignments of the Raman modes of the NaSICON $Na_3Zr_2Si_2PO_{12}$ (N3.0ZSP) obtained from CRYSTAL17 DFT simulations (details of simulations are in Section S1). Note, that there is more than one mode that is assigned to a particular calculated peak. Modes that are indexed in short forms are: translation (t), twisting (or "rotation") (r), symmetric bending (Sb), asymmetric bending (Ab), symmetric stretching (SS), and asymmetric stretching (AS). As an example, t(Na[011]) is a translation of the Na atom (around its position of equilibrium) in the [011] plane within the NaSICON lattice.

Mode	Calc. Freq. (cm^{-1})	Mode Assignment
1	0.0000	Lattice Translation [001]
2	0.0000	Lattice Translation [010]
3	0.0000	Lattice Translation [100]
4	42.7225	t(Na[011]), t(Na[101]), t(Na[110]), r(ZrO_6 [001]), r(PO_4 [001])
5	60.0751	t(Na[001]), t(Na[010]), t(Na[001]), r(ZrO_6 [001])
6	70.5136	t(Na[001]), t(Na[010]), t(Na[001]), r(ZrO_6 [001]), r(PO4 [001])
7	72.6970	t(Na[001]), t(Na[010]), t(Na[001]), r(ZrO_6 [001]), r(SiO_4 [001]), r(PO_4 [001])
8	85.6394	t(Na[001]), t(Na[010]), t(Na[001]), r(ZrO_6 [001])
9	87.3991	t(Na[011]), t(Na[101]), t(Na[110]), r(ZrO_6 [001])
10	98.8880	t(Na[110]), r(ZrO_6 [001]), r(SiO_4 [001]), r(PO_4 [001])
11	110.2935	t(Na[100]), t(Na[111]), r(ZrO_6 [100]), r(ZrO_6 [110]), r(PO_4 [001])
12	122.8619	t(Na[001]), t(Na[111]), r(ZrO_6 [110]), r(SiO_4 [001])
13	129.1409	t(Na[111]), Sb(ZrO_6), r(SiO_4 [001]), r(PO_4 [010])
14	132.4501	t(Na[001]), t(Na[010]), t(Na[001]), Sb(ZrO_6), r(PO_4 [100])
15	134.8279	t(Na[100]), t(Na[010]), Sb(ZrO_6)
16	135.9098	t(Na[100]), t(Na[101]), Sb(ZrO_6)
17	140.2840	t(Na[101]), t(Na[111]), Ab(ZrO_6), r(SiO_4 [010]), r(PO_4 [001])
18	144.9169	t(Na[100]), t(Na[010]), Ab(ZrO_6), r(SiO_4 [010]), r(PO_4 [001])
19	149.8414	t(Na[100]), t(Na[010]), Ab(ZrO6), r(SiO_4 [100]), r(PO_4 [001])
20	150.5651	t(Na[101]), t(Na[011]), Ab(ZrO_6), r(SiO_4 [100]), r(PO_4 [010])
21	154.0060	t(Na[100]), Ab(ZrO_6), r(PO_4 [010])
22	157.8114	t(Na[110]), t(Na[010]), Ab(ZrO_6), r(PO_4 [010])
23	159.9560	t(Na[110]), t(Na[010]), Ab(ZrO_6), r(PO_4 [010])
24	161.3564	t(Na[110]), t(Na[010]), Ab(ZrO_6), r(PO_4 [010])
25	170.0693	t(Na[001]), t(Na[010]), t(Na[001]), Sb(ZrO_6), r(SiO_4 [010]), r(PO_4 [100])
26	172.2209	t(Na[001]), t(Na[010]), t(Na[001]), Sb(ZrO_6)
27	176.9051	t(Na[001]), t(Na[010]), t(Na[001]), Sb(ZrO_6)
28	181.0690	t(Na[001]), t(Na[001]), Sb(ZrO_6)
29	182.3849	t(Na[001]), t(Na[001]), Ab(ZrO_6)
30	187.3536	t(Na[010]), t(Na[001]), Ab(ZrO_6), r(PO_4 [010])
31	189.5056	t(Na[100]), t(Na[001]), Sb(ZrO_6)
32	190.7157	t(Na[001]), t(Na[010]), t(Na[001]), Sb(ZrO_6)

33	196.6156	$Sb(ZrO_6)$
34	203.0153	t(Na[010]), t(Na[001]), $Sb(ZrO_6)$
35	207.2322	t(Na[110]), t(Na[101]), $Ab(ZrO_6)$
36	214.5550	t(Na[100]), t(Na[101]), $Sb(ZrO_6)$
37	227.5714	t(Na[100]), t(Na[101]), $Sb(ZrO_6)$
38	232.8536	t(Na[110]), t(Na[101]), $Sb(ZrO_6)$
39	236.2719	t(Na[110]), t(Na[101]), $Sb(ZrO_6)$
40	239.1998	t(Na[110]), t(Na[101]), $Sb(ZrO_6)$
41	241.3894	t(Na[110]), t(Na[011]), $Sb(ZrO_6)$
42	242.6034	t(Na[110]), t(Na[011]), $Sb(ZrO_6)$
43	245.7663	t(Na[001]), t(Na[010]), $Ab(ZrO_6)$
44	247.9586	t(Na[010]), t(Na[001]), $Sb(ZrO_6)$
45	252.1639	t(Na[101]), t(Na[111]), $Sb(ZrO_6)$
46	265.3784	t(Na[101]), t(Na[111]), $Sb(ZrO_6)$
47	266.3128	t(Na[101]), t(Na[111]), $Sb(ZrO_6)$
48	272.2786	t(Na[101]), t(Na[111]), $Sb(ZrO_6)$
49	274.7554	t(Na[101]), t(Na[111]), $Sb(ZrO_6)$
50	278.3871	t(Na[101]), t(Na[111]), $Sb(ZrO_6)$
51	279.3991	$Sb(ZrO_6)$
52	281.9196	t(Na[101]), t(Na[110]), $Ab(ZrO_6)$
53	286.1608	t(Na[101]), t(Na[110]), $Ab(ZrO_6)$
54	291.6582	t(Na[101]), t(Na[110]), $Ab(ZrO_6)$
55	293.8430	$Ab(ZrO_6)$
56	295.3704	$SS(ZrO_6)$
57	311.4400	$AS(ZrO_6)$
58	311.8728	$AS(ZrO_6)$
59	315.4369	$SS(ZrO_6)$
60	323.9967	$AS(ZrO_6)$
61	326.9914	$AS(ZrO_6)$
62	329.1549	$SS(ZrO_6)$
63	339.3699	$AS(ZrO_6)$
64	340.7982	$AS(ZrO_6)$
65	353.1492	$AS(ZrO_6)$
66	357.7389	$AS(ZrO_6)$
67	372.1270	$AS(ZrO_6)$
68	384.5090	$AS(ZrO_6)$, $Sb(PO_4)$
69	403.8728	$AS(ZrO_6)$, $Sb(SiO_4)$, $Sb(PO_4)$
70	409.3494	$AS(ZrO_6)$, $Sb(SiO_4)$, $Sb(PO_4)$
71	409.6638	$AS(ZrO_6)$, $Sb(SiO_4)$, $Sb(PO_4)$
72	415.4734	$AS(ZrO_6)$, $Sb(SiO_4)$, $Sb(PO_4)$
73	423.5747	$AS(ZrO_6)$, $Sb(SiO_4)$, $Sb(PO_4)$
74	430.7279	$SS(ZrO_6)$, $Sb(SiO_4)$, $Sb(PO_4)$

75	436.9988	SS(ZrO_6), Sb(SiO_4), Sb(PO_4)
76	441.1847	SS(ZrO_6), Sb(SiO_4), Sb(PO_4)
77	455.0415	SS(ZrO_6), Sb(SiO_4), Sb(PO_4)
78	459.9126	SS(ZrO_6), Sb(SiO_4), Sb(PO_4)
79	508.4252	SS(ZrO_6), Sb(SiO_4), Sb(PO_4)
80	510.6596	SS(ZrO_6), Sb(SiO_4), Sb(PO_4)
81	534.9068	SS(ZrO_6), Sb(SiO_4), Sb(PO_4)
82	549.9947	AS(ZrO_6), Sb(SiO_4), Sb(PO_4)
83	552.1295	AS(ZrO_6), Ab(SiO_4), Ab(PO_4)
84	554.3278	AS(ZrO_6), Ab(SiO_4), Ab(PO_4)
85	557.8641	AS(ZrO_6), Ab(SiO_4), Ab(PO_4)
86	568.3046	AS(ZrO_6), Ab(SiO_4), Ab(PO_4)
87	572.1661	AS(ZrO_6), Ab(SiO_4), Ab(PO_4)
88	590.2987	AS(ZrO_6), Ab(SiO_4), Ab(PO_4)
89	601.6567	SS(ZrO_6), Ab(SiO_4), Sb(PO_4)
90	604.7750	AS(ZrO_6), Ab(SiO_4), Ab(PO_4)
91	610.7360	AS(ZrO_6), Ab(SiO_4), Ab(PO_4)
92	627.8206	AS(ZrO_6), Ab(SiO_4), Ab(PO_4)
93	632.0229	AS(ZrO_6), Ab(SiO_4), Ab(PO_4)
94	657.1049	AS(ZrO_6), Ab(SiO_4), Ab(PO_4)
95	658.4068	AS(ZrO_6), Ab(SiO_4), Ab(PO_4)
96	662.2466	AS(ZrO_6), Ab(SiO_4), Sb(PO_4)
97	901.9627	AS(SiO_4)
98	906.6899	AS(SiO_4)
99	907.4195	AS(SiO_4)
100	923.0757	AS(SiO_4)
101	925.0294	AS(SiO_4)
102	925.5833	AS(SiO_4)
103	934.8516	AS(SiO_4)
104	935.4150	AS(SiO_4)
105	951.7611	AS(SiO_4)
106	966.4182	AS(SiO_4), AS(PO_4)
107	975.4268	SS(SiO_4), AS(PO_4)
108	982.3436	AS(SiO_4), AS(PO_4)
109	988.9439	AS(SiO_4), AS(PO_4)
110	994.3543	SS(SiO_4), SS(PO_4)
111	1001.4263	AS(SiO_4), AS(PO_4)
112	1005.2611	AS(SiO_4), AS(PO_4)
113	1022.2902	SS(PO_4)
114	1026.3351	SS(PO_4)
115	1037.9514	SS(PO_4)
116	1052.2416	AS(PO_4)

117	1064.9544	$AS(PO_4)$
118	1146.1995	$AS(PO_4)$
119	1156.6738	$AS(PO_4)$
120	1157.7911	$AS(PO_4)$

Table S8: Assignments of the Raman modes of the impurity *m*-ZrO_2. The interpretation of the modes is identical to what was explained in the description of **Table S7**.

Mode	Calc. Freq. (cm^{-1})	Mode Assignment
1	115.7909	r(ZrO_2 [110])
2	188.3603	Sb(ZrO_2)
3	188.3969	Sb(ZrO_2)
4	202.9186	Ab(ZrO_2)
5	233.0552	Ab(ZrO_2)
6	308.7267	Sb(ZrO_2), Ab(ZrO_2)
7	338.2778	Ab(ZrO_2)
8	345.2735	Ab(ZrO_2)
9	356.0555	Sb(ZrO_2)
10	384.4960	Sb(ZrO_2)
11	385.2649	Ab(ZrO_2)
12	478.5208	Sb(ZrO_2)
13	509.3735	Ab(ZrO_2)
14	545.4148	Sb(ZrO_2)
15	558.7444	Sb(ZrO_2)
16	618.7032	Ab(ZrO_2)
17	646.5437	Ab(ZrO_2)
18	770.7043	SS(ZrO_2)

Table S9: Assignments of the Raman modes of the impurity $Na_2ZrSi_2O_7$. The interpretation of the modes is identical to what was explained in the description of **Table S7.**

Mode	Calc. Freq. (cm^{-1})	Mode Assignment
1	70.8968	t(Na[101]), r(ZrO_6 [110]), r(SiO_4 [011])
2	101.1377	t(Na[110]), t(Na[001]), Sb(ZrO_6), r(SiO_4 [111])
3	118.1890	t(Na[011]), t(Na[111]), r(ZrO_6 [010]), r(SiO_4 [101])
4	120.2545	t(Na[100]), t(Na[110]), r(ZrO_6 [010]), r(SiO_4 [010])
5	129.2724	t(Na[111]), t(Na[110]), Ab(ZrO_6), r(SiO_4 [101])
6	132.2174	t(Na[100]), Ab(ZrO_6), r(SiO_4 [001])
7	158.1131	t(Na[100]), t(Na[011]), Ab(ZrO_6), r(SiO_4 [001])
8	160.5500	t(Na[100]), t(Na[011]), Ab(ZrO_6), r(SiO_4 [011])
9	169.2149	t(Na[110]), t(Na[111]), Ab(ZrO_6), r(SiO_4 [011])
10	183.3230	t(Na[100]), Ab(ZrO_6), r(SiO_4 [110])
11	199.1171	t(Na[100]), (Na[110]), Ab(ZrO_6), r(SiO_4 [101])
12	221.4612	t(Na[001]), Ab(ZrO_6), Sb(ZrO_6), r(SiO_4 [101])
13	241.6159	t(Na[010]), Ab(ZrO_6), r(SiO_4 [101])
14	248.2759	t(Na[010]), Ab(ZrO_6), r(SiO_4 [101])
15	258.8266	t(Na[010]), Ab(ZrO_6), r(SiO_4 [101])
16	269.5954	Ab(ZrO_6), r(SiO_4 [101])
17	320.0136	Sb(ZrO_6), r(SiO_4 [110])
18	341.1943	Ab(ZrO_6), r(SiO_4 [111])
19	357.4132	Ab(ZrO_6), Sb(SiO_4)
20	390.1828	Sb(ZrO_6), Sb(SiO_4)
21	393.4126	Sb(ZrO_6), Sb(SiO_4)
22	419.2195	SS(ZrO_6), Sb(SiO_4)
23	439.7868	Ab(ZrO_6), Sb(SiO_4)
24	503.2211	SS(ZrO_6), Sb(SiO_4)
25	536.1329	Ab(ZrO_6), SS(ZrO_6), Sb(SiO_4)
26	548.8925	SS(ZrO_6), Sb(SiO_4)
27	607.8885	AS(ZrO_6), Sb(SiO_4)
28	629.8697	AS(ZrO_6), Sb(SiO_4)
29	732.9464	SS(SiO_4)
30	869.8617	SS(SiO_4)
31	924.3959	AS(SiO_4)
32	956.0871	AS(SiO_4)
33	958.7309	AS(SiO_4)
34	1005.9236	AS(SiO_4)
35	1011.8602	AS(SiO_4)
36	1049.8196	AS(SiO_4)

Figure S10: Experimental Raman spectra of *m*-ZrO_2 obtained within the range of 100 cm^{-1} to 1000 cm^{-1}. The experimental Raman spectrum of *m*-ZrO_2 (in green) matches well with DFT calculations (in light blue sticks). DFT calculations are simultaneously used to identify peaks in the NaSICON samples. The other sticks are the N3.0ZSP DFT calculation (magenta) and $Na_2ZrSi_2O_7$ (maroon), calculated and indexed in Table S7 and S9 respectively.

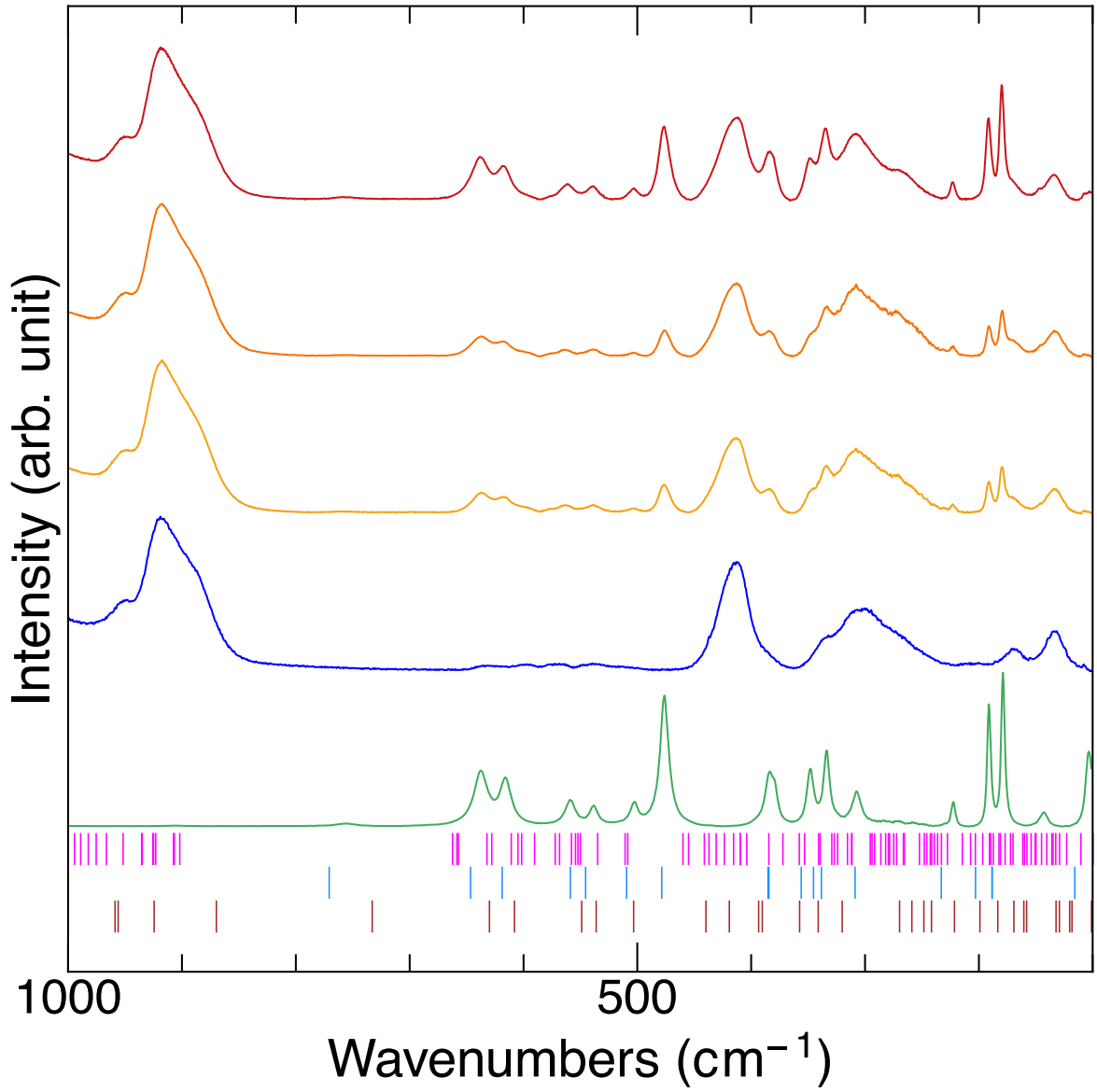

Table S11: Basis sets of Na, Zr, Si, P, and O used in the calculation using CRYSTAL17 for the compounds reported in **Tables S7 - S9**.

Na	**Zr**
11 9 0 0 7 2.0 1.0 26041.1099270 0.00061806342811 3906.12685480 0.00477486044140 888.974549930 0.02447168482900 251.454979610 0.09475539497700 81.6501435120 0.26867496920000 28.9041584010 0.47925475440000 10.6257829320 0.33248591469000 0 0 3 2.0 1.0 53.7694101790 0.01952773187200 16.3082430250 0.09264801079400 2.37303841250 -0.39938670172000 0 0 2 1.0 1.0 0.95730772603 1.64285953910000 0.40806460959 0.55692596966000 0 0 1 0.0 1.0 0.42460191000 1.00000000000000 0 0 1 0.0 1.0 0.12055549000 1.00000000000000 0 2 5 6.0 1.0 138.079799890 0.00579518919290 32.2327003930 0.04162084625100 9.98160753600 0.16281916885000 3.48220339280 0.36011784647000 1.22991346200 0.44858979889000 0 2 1 0.0 1.0 0.40094322000 1.00000000000000 0 2 1 0.0 1.0 0.12067345000 1.00000000000000 0 3 1 0.0 1.0 0.30530000000 1.00000000000000	240 11 INPUT 12. 0 2 4 4 2 0 8.636528 150.242994 0 3.717639 18.780036 0 7.626728 33.192791 0 7.453207 66.389039 0 3.358389 4.620726 0 3.229738 9.260270 0 5.938086 13.993383 0 5.825544 20.995882 0 2.205019 2.285166 0 2.206292 3.441260 0 4.800215 -5.239320 0 4.798992 -6.987424 0 0 0 2 2 1.0 11.0000000000 -0.190755952570 9.50000000000 0.338955887540 0 0 1 2 1.0 3.91891211000 1.000000000000 0 0 1 0 1.0 1.48625300000 1.000000000000 0 0 1 0 1.0 0.581428600000 1.000000000000 0 2 4 6 1.0 8.60663055430 0.040404260236 4.44009799580 -0.211877452010 1.12810269460 0.491642668910 0.54346076310 0.573033706580 0 2 1 0 1.0 0.49792620000 1.000000000000 0 2 1 0 1.0 0.16451000000 1.000000000000 0 3 3 2 1.0 4.55679577950 -0.009619056902 1.29049397970 0.205699901550 0.51646987222 0.418313818510 0 3 1 0 1.0 0.38034710000 1.000000000000 0 3 1 0 1.0 0.16106300000 1.000000000000 0 4 1 0 1.0 0.34548200000 1.000000000000
Si	**P**
14 10	15 10

0 0 7 2.0 1.0	
44773.358078	0.00055914765868
6717.1992104	0.00432060401890
1528.8960325	0.02218709646000
432.54746585	0.08648924911600
140.61505226	0.24939889716000
49.857636724	0.46017197366000
18.434974885	0.34250236575000
0 0 3 2.0 1.0	
86.533886111	0.02130006300700
26.624606846	0.09467613931800
4.4953057159	-0.32616264859000
0 0 2 2.0 1.0	
2.1035045710	1.39808038500000
1.3106094922	0.63865786699000
0 0 1 0.0 1.0	
0.5422443800	1.00000000000000
0 0 1 0.0 1.0	
0.1460762500	1.00000000000000
0 2 5 6.0 1.0	
394.47503628	0.00262856939590
93.137683104	0.02055625774900
29.519608742	0.09207026280100
10.781663791	0.25565889739000
4.1626574778	0.42111707185000
0 2 1 2.0 1.0	
1.4499318500	1.00000000000000
0 2 1 0.0 1.0	
0.4949286700	1.00000000000000
0 2 1 0.0 1.0	
0.1346786100	1.00000000000000
0 3 1 0.0 1.0	
0.3074090300	1.00000000000000

0 0 7 2.0 1.0	
52426.999233	0.0005520716410
7863.2660552	0.0042678595308
1789.5227333	0.0219315291860
506.27300165	0.0856671683730
164.60698546	0.2484068660500
58.391918722	0.4633675397100
21.643663201	0.3535055815600
0 0 3 2.0 1.0	
99.013837620	0.0218956799580
30.550439817	0.0956504702950
5.4537087661	-0.2945427018600
0 0 2 2.0 1.0	
2.6503362563	1.3294381200000
1.2726688867	0.6610939647300
0 0 1 0.0 1.0	
0.3072409700	1.0000000000000
0 0 1 0.0 1.0	
0.1202708300	1.0000000000000
0 2 5 6.0 1.0	
472.27219248	0.0025710623052
111.58882756	0.0202502979990
35.445936418	0.0915807167870
12.990776875	0.2574945401400
5.0486221658	0.4286289975800
0 2 1 3.0 1.0	
1.8889755200	1.0000000000000
0 2 1 0.0 1.0	
0.4424064200	1.0000000000000
0 2 1 0.0 1.0	
0.1573225300	1.0000000000000
0 3 1 0.0 1.0	
0.5061295000	1.0000000000000

O	
8 8	
0 0 6 2.0 1.0	
27032.382631	0.00021726302465
4052.3871392	0.00168386621990
922.32722710	0.00873956162650
261.24070989	0.03523996880800
85.354641351	0.11153519115000
31.035035245	0.25588953961000
0 0 2 2.0 1.0	
12.260860728	0.39768730901000
4.9987076005	0.24627849430000
0 0 1 0.0 1.0	
1.0987136000	1.00000000000000
0 0 1 0.0 1.0	
0.3565870100	1.00000000000000
0 2 4 4.0 1.0	
63.274954801	0.0060685103418
14.627049379	0.0419125758240
4.4501223456	0.1615384108800
1.5275799647	0.3570695131100
0 2 1 0.0 1.0	
0.5489735000	1.0000000000000
0 2 1 0.0 1.0	
0.1858671100	1.0000000000000

0 3 1 0.0 1.0 0.4534621300 1.0000000000000	

S7 Grain size distribution from SEM imaging

Figure S12: Statistical distribution of the cross-section grain size of L15 (b) and L0 (d). The mean average grain area for L15 is around 0.093 μm^2, with a maximum grain area of 17.18 μm^2. The sampled cross section of L0 has an average grain area of 0.372 μm^2, with a maximum grain area of 39.53 μm^2.

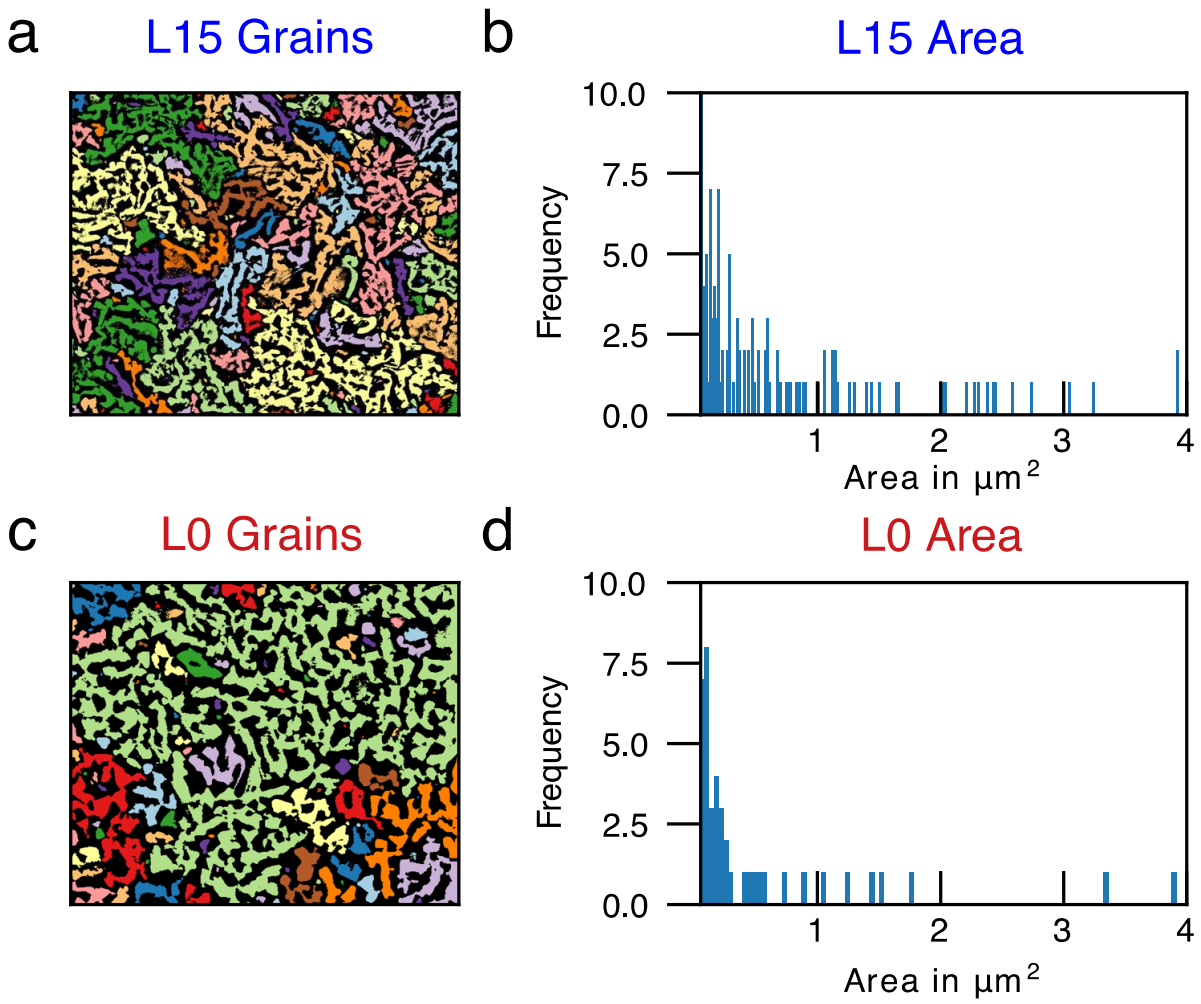

Figure S13: SEM images of pre-sintered powders, after calcination and ball milling of samples: a) L0, b) L5, c) L10, and d) L15, respectively. The black background in these micrographs is the carbon tape used as an adhesive for the pre-sintered powders.

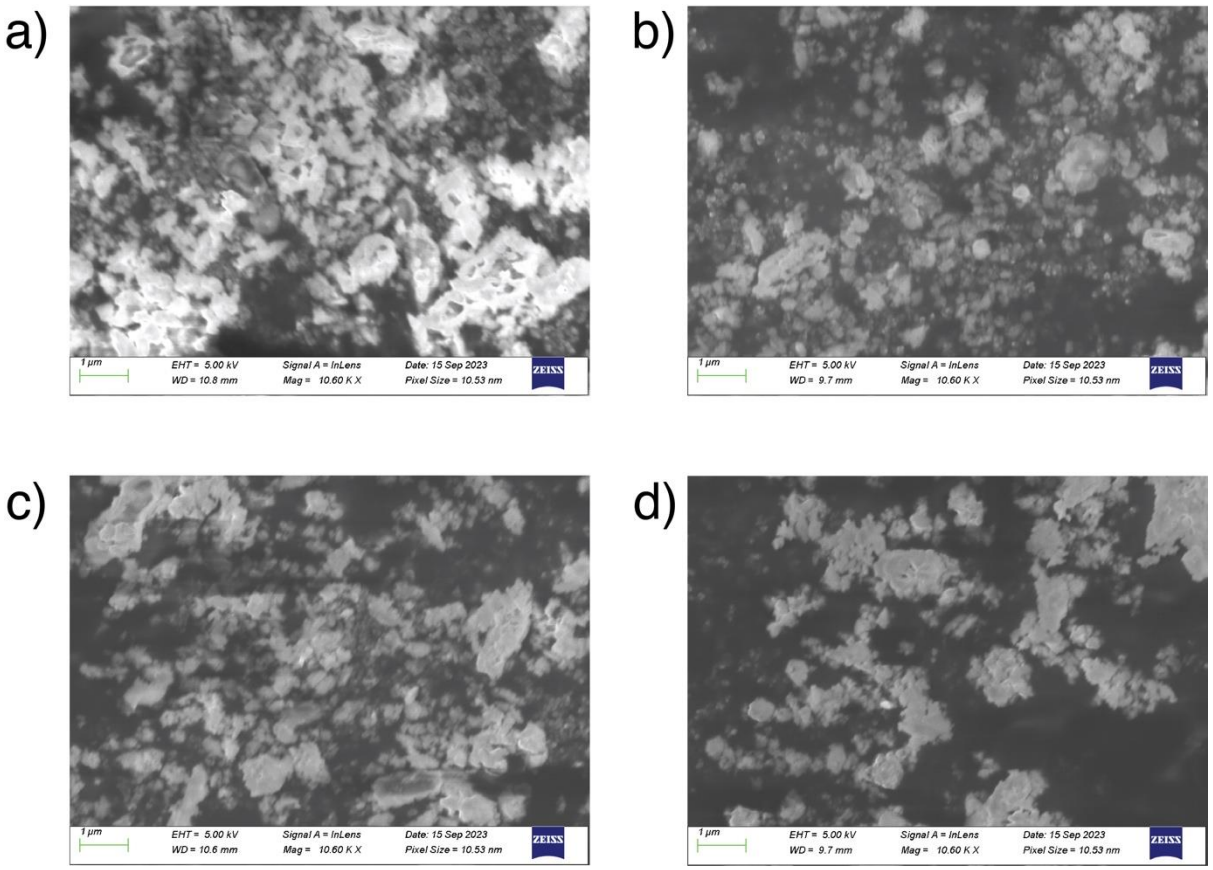

Table S14: Maximum and average grain area (in μm^2) detected in the SEM micrographs using the method exposed in Ref. 32 of the main text.

Species	Maximum grain area	Average grain area
L0	10.647	0.0316
L5	3.492	0.0100
L10	3.504	0.0136
L15	7.250	0.0079

S8 Fitting Parameters of Impedance Spectroscopy, electronic conductivity, and symmetric battery performance

Figure S15: Comparison of L0 and L15 NaSICON pellet at low-temperature EIS measurement, at 193 K. (a) shows the overall Nyquist plots containing L0 (dark red) and L15 (blue). The L15 is barely visible, showing the large resistance experienced by the Na-ion during ion transport at 193 K in L0 compared to L15. (b) shows the zoomed-in graph, near the origin of (a), where the bulk resistance of L0 is visible. The L0 pellet has a dimension of 8.15 mm in diameter and 1.90 mm in thickness. The equivalence circuit of L0 is also shown here. All Nyquist plots here are fitted, indicated with their respective dashed line.

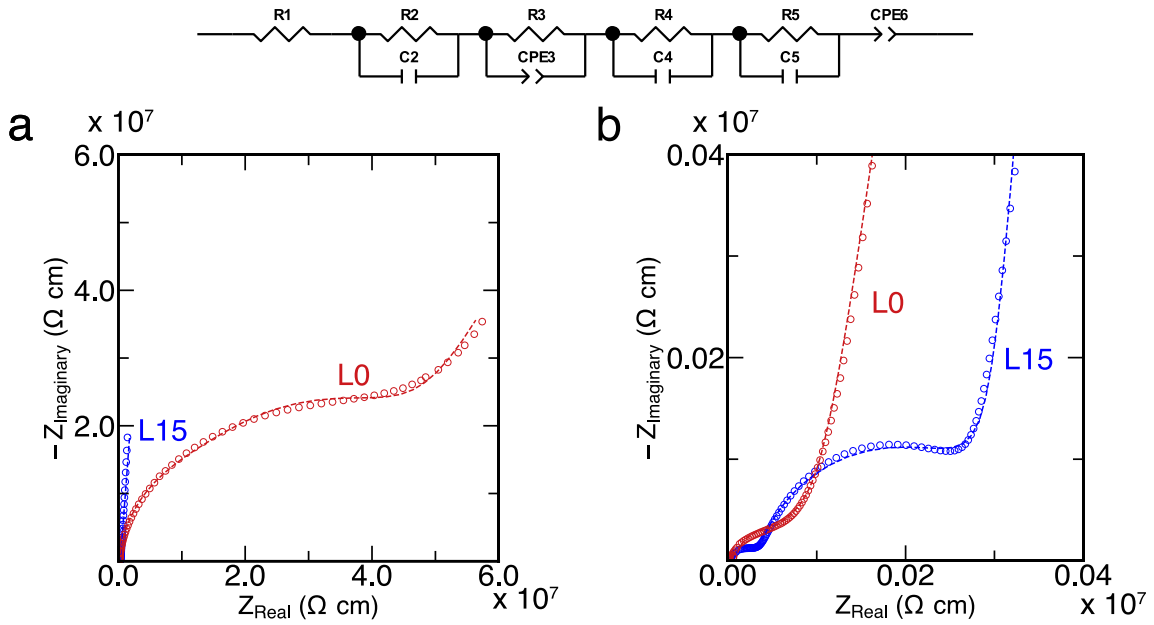

Figure S16: Charge/discharge profile between 0 – 3 V of two all-NaSICON solid-state cells with the following configurations: a) $Na_3V_2(PO_4)_3$ | NZSP-L0 | $Na_3V_2(PO_4)_3$ and b) $Na_3V_2(PO_4)_3$ | NZSP-L15 | $Na_3V_2(PO_4)_3$, with a charge/discharge rate of C/20 (blue), C/10 (green) and C/5 (yellow). The x-axis represents the specific capacity in mAh g^{-1}, while the y-axis denotes the cell voltage of the battery. c), d) and e) shows the polarization of L0 (yellow) and L15 (blue) during the charging/discharge process, from 0 – 3 V. In panels c), d), and e). The x-axis presents the amount of Na per formula unit x in the active material $Na_xV_2(PO_4)_3$ during the charge/discharge process.

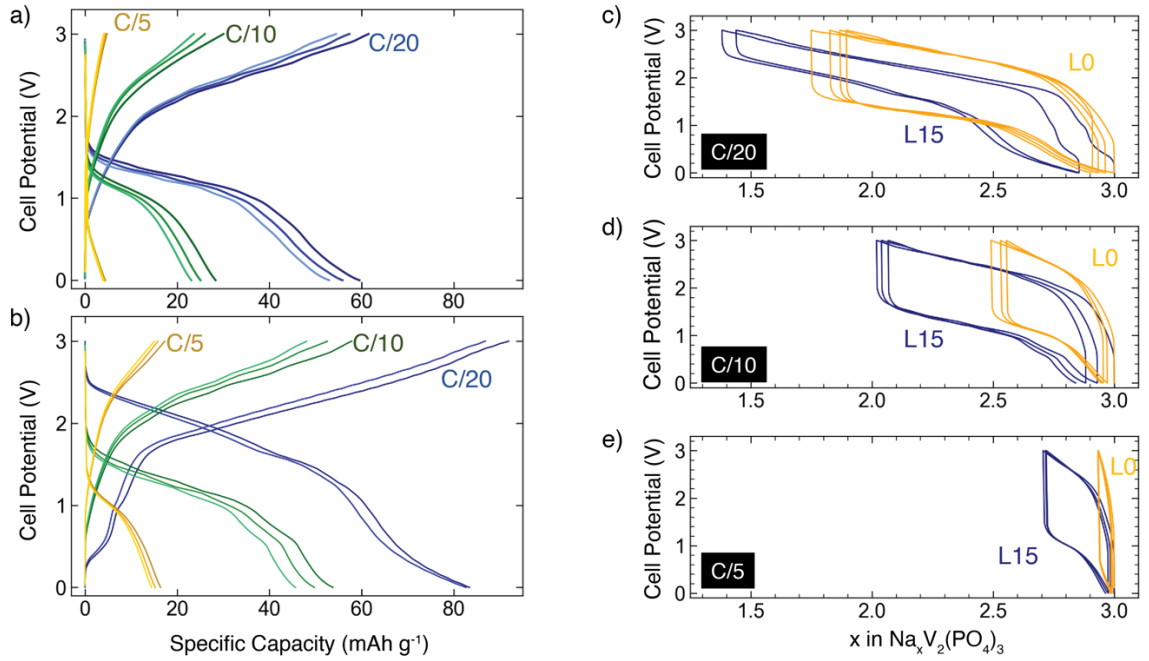

Table S17: Gravimetric capacity (in mAh g^{-1}) of the first charge at C/20, C/10, and C/5 for L0 and L15 sample and their corresponding estimated polarization values (in V).

Rate	**C/20**		**C/10**		**C/5**	
Sample	**Capacity**	**Polarization**	**Capacity**	**Polarization**	**Capacity**	**Polarization**
NZSP-L0	61.49	1.31	30.01	1.50	4.70	2.22
NZSP-L15	91.94	0.62	57.90	1.27	17.31	1.63

Figure S18: Optical photographs of the a) L15 pellet with gold sputtered on the surface, b) a close-up image of the NVP | L15 | NVP cell, and c) the electrochemical setup of our NVP | L15 | NVP cell.

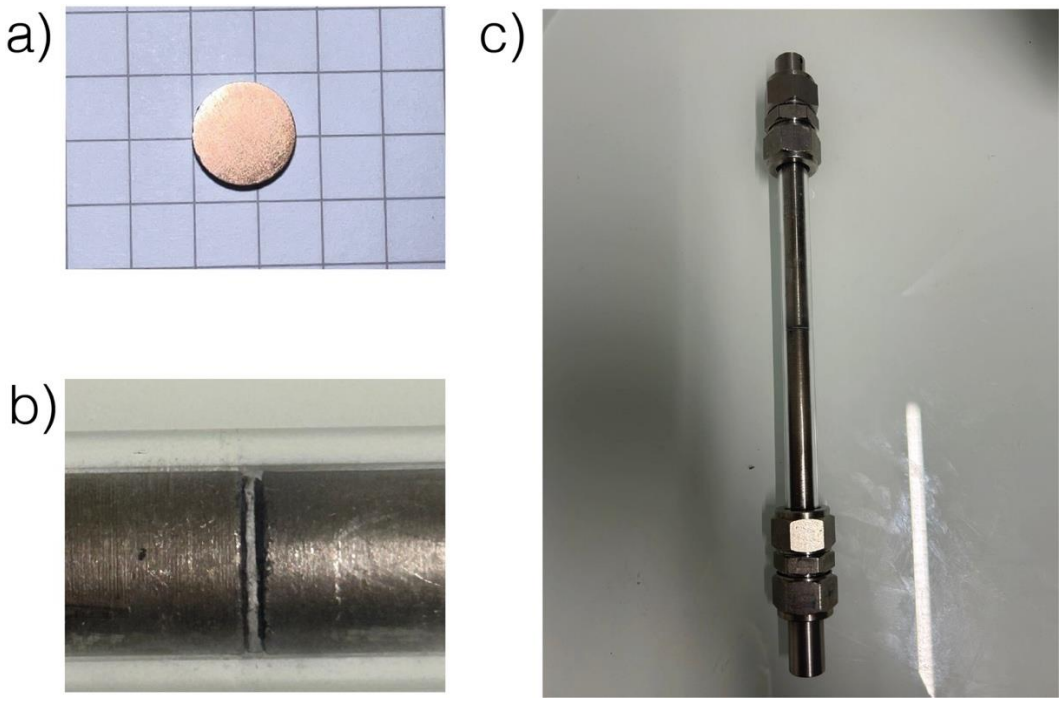

Table S19: Fitted parameters of the Nyquist plot of **Figure 4a** in the main text. The various values of the equivalence circuit used to fit the Nyquist plot at 193 K are reported in this table, along with its associated error. R element is a resistor, and CPE is a constant phase element modeling the pseudo-capacitance experienced by the bulk and grain boundary in the Nyquist plot.

Circuit Element	Fitted value	Error (%)
R1 (Ω)	3066	8.20
R2 (Ω)	1.09×10^{4}	4.69
CPE2 (F)	2.99×10^{-11}	43.31
R3 (Ω)	1.18×10^{5}	2.65
CPE3 (F)	4.31×10^{-9}	11.85
CPE4 (F)	2.08×10^{-8}	9.11

Figure S20: DC polarization test at a constant voltage of 1 Volt over a period of 8 hours of the L15 pellet. A smaller inset shows the rapid decrease of current at the beginning of the experiment to achieve a steady state, indicating the low electronic conductivity. The electronic transference number is ~1.57 x 10^{-5}.

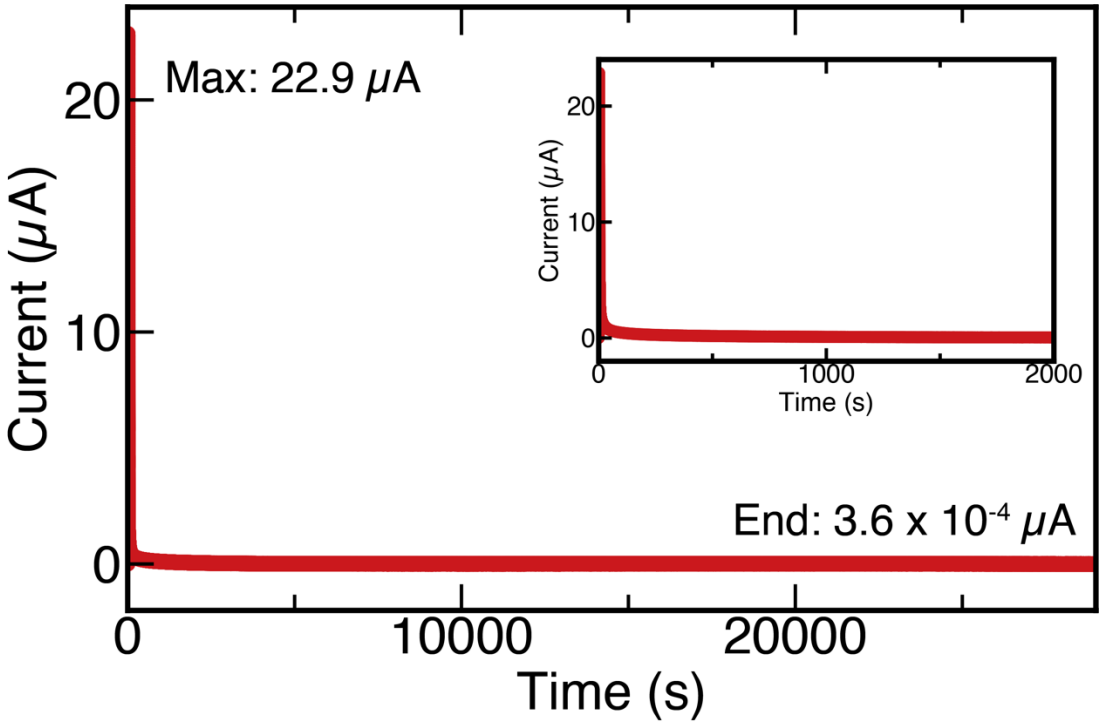

Table S21: Fitted parameters of the Nyquist plot of L0 at 193 K (see **Figure S15**). The various values of the equivalence circuit used to fit the Nyquist plot at 193 K are reported in this table, along with its associated error. R element is a resistor, C is a capacitor, and CPE is a constant phase element modeling the pseudo-capacitance experienced by the bulk and grain boundaries in the Nyquist plot.

Circuit Element	Fitted value	Error (%)
R1 (Ω)	3263	5.87
R2 (Ω)	1.16×10^{4}	8.33
C2 (F)	2.40×10^{-11}	6.84
R3 (Ω)	1.69×10^{4}	11.99
CPE3 (F)	1.71×10^{-9}	58.27
R4 (Ω)	4.48×10^{6}	3.99
C4 (F)	8.99×10^{-10}	1.87
R5 (Ω)	9.88×10^{6}	1.87
C4 (F)	1.92×10^{-9}	4.04
CPE6 (F)	2.14×10^{-8}	1.27

References

[1] F. Lalère *et al.*, “Improving the energy density of $Na_3V_2(PO_4)_3$-based positive electrodes through V/Al substitution,” *Journal of Materials Chemistry A*, vol. 3, no. 31, pp. 16198–16205, 2015.

[2] F. Fauth, I. Peral, C. Popescu, and M. Knapp, “The new material science powder diffraction beamline at Alba Synchrotron,” *Powder Diffraction*, vol. 28, no. S2, 2013.

[3] J. Rodriguez-Carvajal, “FULLPROF: a program for Rietveld refinement and pattern matching analysis,” in *satellite meeting on powder diffraction of the XV congress of the IUCr*, 1990, vol. 127.

[4] R. Dovesi, A. Erba, R. Orlando, C. M. Zicovich-Wilson, B. Civalleri, L. Maschio, M. Rérat, S. Casassa, J. Baima, S. Salustro, and B. Kirtman, “Quantum-mechanical condensed matter simulations with Crystal,” *WIREs Computational Molecular Science*, vol. 8, no. 4, 2018.

[5] R. Dovesi, C. Roetti, C. Freyria-Fava, M. Prencipe, and V. R. Saunders, “On the elastic properties of lithium, sodium and potassium oxide. an ab initio study,” *Chemical Physics*, vol. 156, no. 1, pp. 11–19, 1991.

[6] R. Nada, J. B. Nicholas, M. I. McCarthy, and A. C. Hess, “Basis sets for Ab Initio Periodic Hartree-Fock Studies of zeolite/adsorbate interactions: He, Ne, and Ar in silica sodalite,” *International Journal of Quantum Chemistry*, vol. 60, no. 4, pp. 809–820, 1996.

[7] P. J. Hay and W. R. Wadt, “ab initio effective core potentials for molecular calculations. potentials for K to au including the outermost core orbitals,” *The Journal of Chemical Physics*, vol. 82, no. 1, pp. 299–310, 1985.

[8] T. Bredow and M. Lerch, “Anion distribution in Zr_2ON_2,” *Zeitschrift für anorganische und allgemeine Chemie*, vol. 630, no. 13–14, pp. 2262–2266, 2004.

[9] C. Adamo and V. Barone, “Toward reliable density functional methods without adjustable parameters: The PBE0 model,” *The Journal of Chemical Physics*, vol. 110, no. 13, pp. 6158–6170, 1999.

[10] M. Ferrero, M. Rérat, R. Orlando, and R. Dovesi, “Coupled perturbed Hartree-Fock for periodic systems: The role of symmetry and related computational aspects,” *The Journal of Chemical Physics*, vol. 128, no. 1, p. 014110, 2008.

[11] M. Ferrero, M. Rérat, R. Orlando, and R. Dovesi, “The calculation of Static Polarizabilities of 1-3D periodic compounds. the implementation in the crystal code,” *Journal of Computational Chemistry*, vol. 29, no. 9, pp. 1450–1459, 2008.

[12] M. Ferrero, M. Rérat, B. Kirtman, and R. Dovesi, “Calculation of First and second static hyperpolarizabilities of one- to three-dimensional periodic compounds. implementation in the crystal code.,” *The Journal of Chemical Physics*, vol. 129, no. 24, p. 244110, 2008.